ELSEVIER

Nuclear Instruments and Methods in Physics Research A 434 (1999) 90–102

NUCLEAR INSTRUMENTS & METHODS IN PHYSICS RESEARCH Section A

www.elsevier.nl/locate/nima

# Charge transport in non-irradiated and irradiated silicon detectors

C. Leroy[a,*], P. Roy[a], G.L. Casse[b], M. Glaser[b], E. Grigoriev[b], F. Lemeilleur[b]

[a]*Lab. de Phys. Nucl., Université de Montréal, C.P. 6128, Succursale Centre-Ville, Montréal (Québec), Canada H3C 3J7*
[b]*CERN, Geneva, Switzerland*

**Abstract**

A model describing the transport of the charge carriers generated in n-type silicon detectors by ionizing particles is presented. In order to reproduce the experimental current pulse responses induced by α and β particles in non-irradiated and irradiated detectors up to fluences ($\Phi$) much beyond the n to p-type inversion, an n-type region 15 μm deep is introduced on the $p^+$ side of the diode. This model also gives mobilities which decrease linearly up to fluences of around $5 \times 10^{13}$ particles/cm$^2$ and beyond, converging to saturation values of about 1000 and 450 cm$^2$/V s for electrons and holes, respectively. The charge carrier lifetime degradation with increased fluence, due to trapping, is responsible for a predicted charge collection deficit for β particles and for α particles which is found to agree with direct CCE measurements. 

## 1. Introduction

The electrical characteristics of n-type silicon detectors as a function of particle fluence ($\Phi$) can be extracted by modelling the transport of the charge carriers generated by α or β particles in non-irradiated and irradiated silicon detectors [1]. The model is used to fit the experimental signal-current pulse response (measured as a function of the collection time) induced by α and β particles in $p^+$–n–$n^+$ diodes. The extracted electrical characteristics of a $p^+$–n–$n^+$ diode are the effective impurity or dopant concentrations ($N_{eff}$), the electron ($\mu_e$) and hole ($\mu_h$) mobilities, and the charge carrier lifetimes ($\tau_{te}$, $\tau_{th}$).

## 2. Charge transport model

The electrical characteristics are extracted by solving in one dimension (through the use of a transverse diffusion term), a system of five partial differential equations (cf. Ref. [1] for more details): the current continuity equations for electrons and holes, the Poisson equation (which determines the electric field and takes account of plasma effects) and two equations relating the concentration of trapped to untrapped charges. A planar semiconductor ($p^+$–n–$n^+$ diode) is considered (Fig. 1), with the ohmic side and the junction side located at $x = 0$ and $x = w$, respectively. When neglecting the

* Corresponding author. Tel.: + 1-514-343-5837; fax: + 1-514-343-6215.

*E-mail address:* claude.leroy@cern.ch (C. Leroy)

0168-9002/99/$ - see front matter 
PII: S0168-9002(99)00437-4

size of the $p^+$ and $n^+$ regions, the integration of the one-dimensional Poisson's equation at $t = 0$, for a simple, abrupt pn junction operated in overdepleted mode ($V_b > V_d$), gives

$$E(x,0) = -\frac{qN_{eff}}{\varepsilon}x + \frac{V_b}{w} + \frac{V_d N_{eff}}{w|N_{eff}|} \quad \text{for } 0 < x < w \tag{1}$$

$$E(0,t) = E(w,t) = 0 \tag{2}$$

$$\psi(0,t) = V_0 + \psi_p \approx 0 \quad \text{and} \quad \psi(w,t) = \psi_p - V_b \approx -V_b \tag{3}$$

where $\psi$ and $E$ are the electrostatic potential and the electric field, respectively; $q, \varepsilon$ and $w$ are the electron charge, the permittivity and the thickness of the diode, respectively; $V_0 \approx 0.6$ V is the built-in voltage, $V_b$ the applied bias voltage, $\psi_p \approx -0.3$ V the electrostatic potential of the neutral p-type region and $V_d$ the full depletion bias voltage.

The drift velocity of the charge carriers reaches a saturation value $v_s$ for electric field values around $10^4$ V/cm. The empirical equation describing the mobility as a function of the electric field is

$$\mu(x) = \frac{\mu_0}{[1 + (\mu_0 E(x)/v_s)^m]^{1/m}} \tag{4}$$

where $\mu_0$ is the zero field mobility, $m = 1$ for holes, $m = 2$ for electrons; $v_s = 1.05 \times 10^7$ and $10^7$ cm/s for electrons and holes, respectively.

The mobilities are also dependent on the temperature and dopant concentrations. Changing the temperature by 1.5°C changes both mobilities by $\approx 1\%$. In the present work, all the measurements using α particles and several using β particles were performed at room temperature (22°C), while the measurements using β particles for detectors P88, P189 and P304 were made at 15°C. The temperature and the dopant concentration dependence of mobility is taken into account via the empirical equation

$$\mu(T, N_{eff}) = \mu_{min} + \frac{\mu_0 (T/300)^v - \mu_{min}}{1 + (T/300)^\xi (N_{eff}/N_{ref})^\alpha} \tag{5}$$

where the values used for the electrons (holes) are: $\mu_{min} = 55.24$ (49.7) $\text{cm}^2/\text{V s}$, $N_{ref} = 1.072 \times 10^{17}$ ($1.606 \times 10^{17}$) dopant atoms/$\text{cm}^3$, $v = -2.3$ ($-2.2$), $\xi = -3.8$ ($-3.7$), $\alpha = 0.73$ (0.70), $T$ is the temperature in Kelvin and $\mu_0$ is the mobility at $T = 300$ K. The temperature dependence of mobility is shown in Fig. 2 using $\mu_0$(for e) = 1350 $\text{cm}^2/\text{V s}$ and $\mu_0$(for h) = 480 $\text{cm}^2/\text{V s}$ at $T = 300$ K.

In the absence of an analytical solution to the system of the five partial differential equations, the equations are discretized using Gummel's decoupling scheme [2] to obtain a numerical solution [1]. The observed signal ($V(t)$) is a convolution of the current ($I(t)$ obtained from Ramo's theorem [3]) produced by all the individual charge carriers and the response of the system, which is simply an RC circuit. The response of the system is a Gaussian with a characteristic time constant $\sigma = R_a C$, where $C$ is the capacitance of the detector and $R_a = 50\ \Omega$ the input impedance of the amplifier:

$$I(t) = \frac{18 D_a t + r_0^2}{w r_0^2} \int_0^w (\mu_e n + \mu_h p) E \, dx \tag{6}$$

$$V(t) = \frac{G R_a}{\sigma\sqrt{2\pi}} \sum_{e,h} \int_{-\infty}^{\infty} I(t') \exp\left( -\frac{(t - t')^2}{2\sigma^2} \right) dt' \tag{7}$$

where $D_a$ is the ambipolar diffusion constant, $G = 1000$ the gain of the amplifier and $r_0$ the initial radius of the column of deposited charge.

The quantities of interest are extracted using the code MINUIT [4] to minimize the $\chi^2$ obtained from fitting the numerical solutions found for $V(t)$ to the measured current pulse response induced by α particles from an $^{241}$Am source with an α energy of 5.49 MeV and β particles from a $^{106}$Ru source with an energy $> 2$ MeV, selected by an external trigger. The current pulses induced by particles penetrating the silicon diode are detected by a fast current amplifier. The pulses are recorded by a LeCroy digital oscilloscope, used in averaging mode, to improve the signal-to-noise ratio [5,6]. A summary of the characteristics, at $\Phi = 0$, of the standard float zone silicon detectors used in the present work is given in Table 1.

### 2.1. Non-irradiated detectors ($\Phi = 0$)

Fits of the charge carrier transport model to the current pulses induced by relativistic electrons and

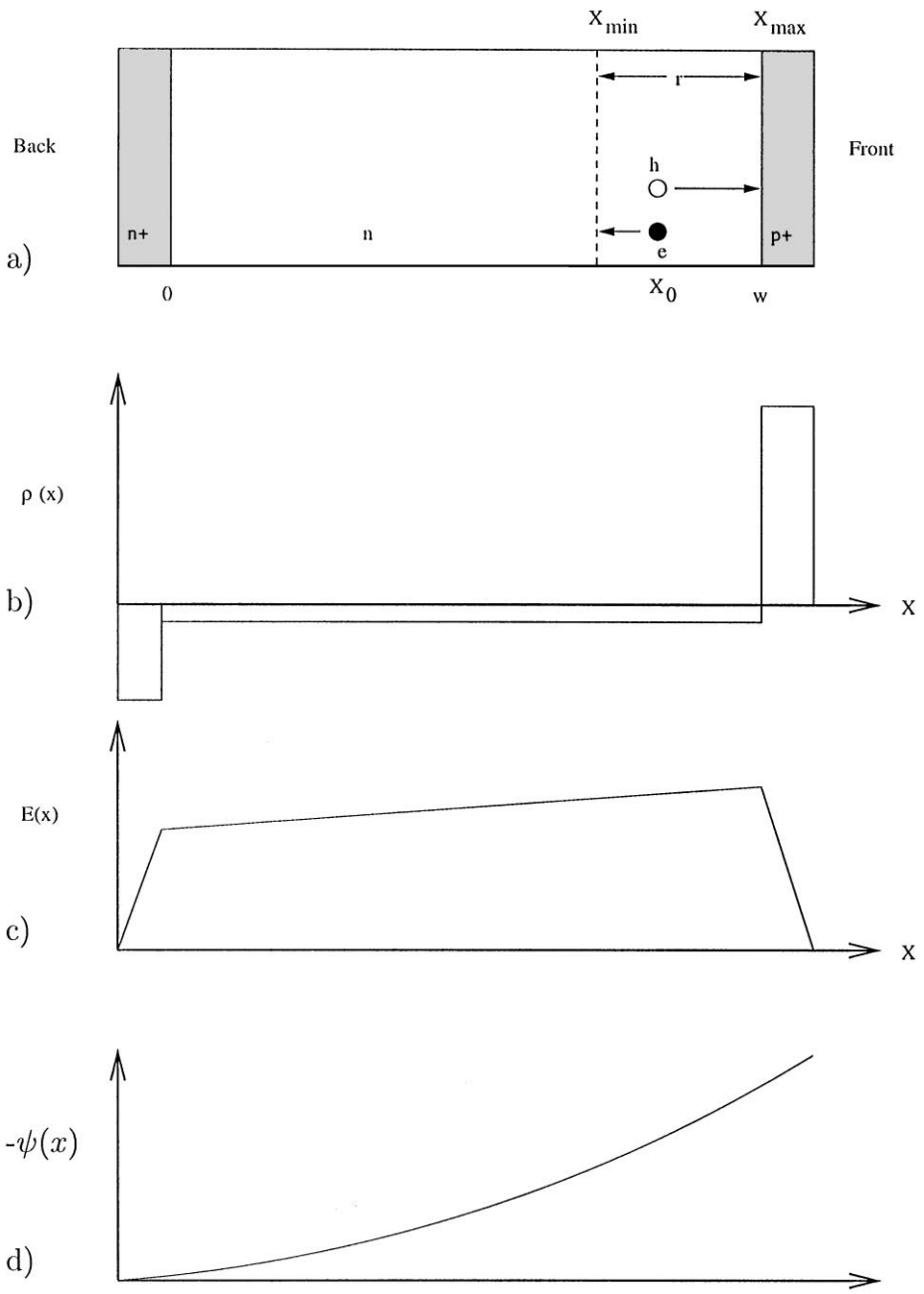


Fig. 1. (a) Representation of a $p^+$–n–$n^+$ diode, (b) the dopant profile ($\rho$), (c) the electric field ($E$) and (d) the electrostatic potential ($\psi$).

by α particles incident either on the front side or the back side of non-irradiated detectors ($\Phi = 0$) reproduce well the shape of the measured current pulses (α and β) as shown in Fig. 3 (for detectors M25 and M50 as examples). The model also gives the values of the electron and hole mobilities reported in Table 2. The average mobilities achieved for electrons and holes at $\Phi = 0$ for the detectors described

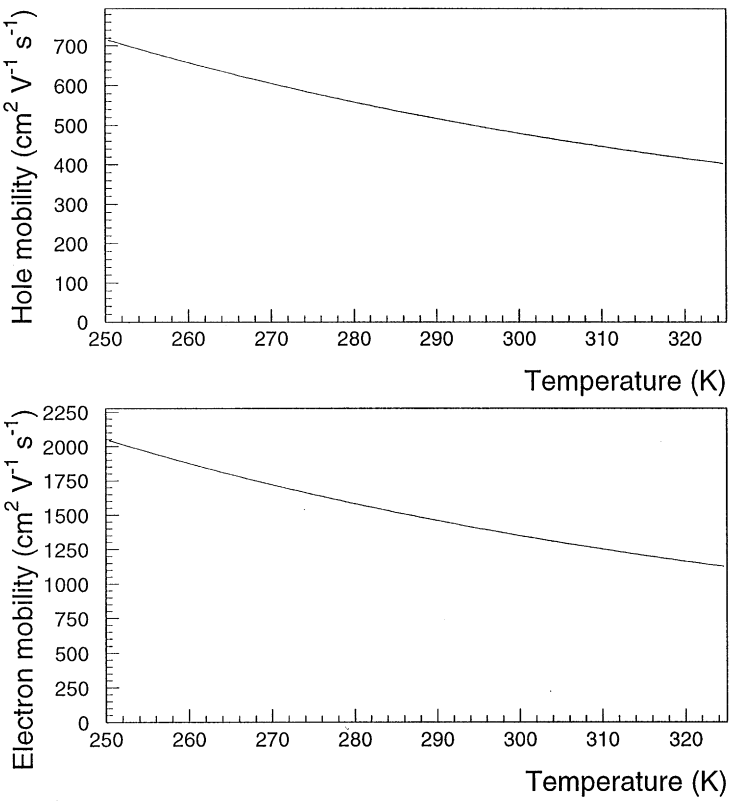


Fig. 2. Effect of the temperature on the mobilities (according to Eq. (5), with $\mu_0$(for e) = 1350 cm$^2$/V s and $\mu_0$(for h) = 480 cm$^2$/V s at $T = 300$ K).

Table 1
Characteristics at $\Phi = 0$ of the standard float zone detectors used in the present work. The detectors have been irradiated by steps of fluence from $\Phi = 0$ up to $9.92 \times 10^{13}$ n/cm$^2$ for M4, up to $7.5 \times 10^{13}$ p/cm$^2$ for M18, M25, M35, and up to $28.7 \times 10^{13}$ p/cm$^2$ for P88, P189 and P304. M49, M50, M53 were not irradiated

| Detector | Current pulse source | Thickness (μm) | $N_{eff}$ ($\times 10^{11}$ cm$^{-3}$) | $\rho$ (kΩ cm) | Maximum fluence (cm$^{-2}$) |
|---|---|---|---|---|---|
| M4 (1 cm$^2$) | α | 317 | − 3.4 | 12.2 | $9.92 \times 10^{13}$ n |
| M18 (1 cm$^2$) | α, β | 309 | − 4.1 | 11 | $7.5 \times 10^{13}$ p |
| M25 (1 cm$^2$) | α, β | 308 | − 2.1 | 23 | $7.5 \times 10^{13}$ p |
| M35 (1 cm$^2$) | α | 508 | − 1.7 | 24 | $7.5 \times 10^{13}$ p |
| M49 (1 cm$^2$) | β | 301 | − 4.7 | 8.9 | — |
| M50 (1 cm$^2$) | β | 471 | − 1.8 | 22.8 | — |
| M53 (1 cm$^2$) | β | 223 | − 5.4 | 7.7 | — |
| P88 (0.25 cm$^2$) | α, β | 290 | − 18 | 2.5 | $28.7 \times 10^{13}$ p |
| P189 (0.25 cm$^2$) | α, β | 294 | − 18 | 2.5 | $28.7 \times 10^{13}$ p |
| P304 (0.25 cm$^2$) | α, β | 320 | − 7 | 6 | $28.7 \times 10^{13}$ p |

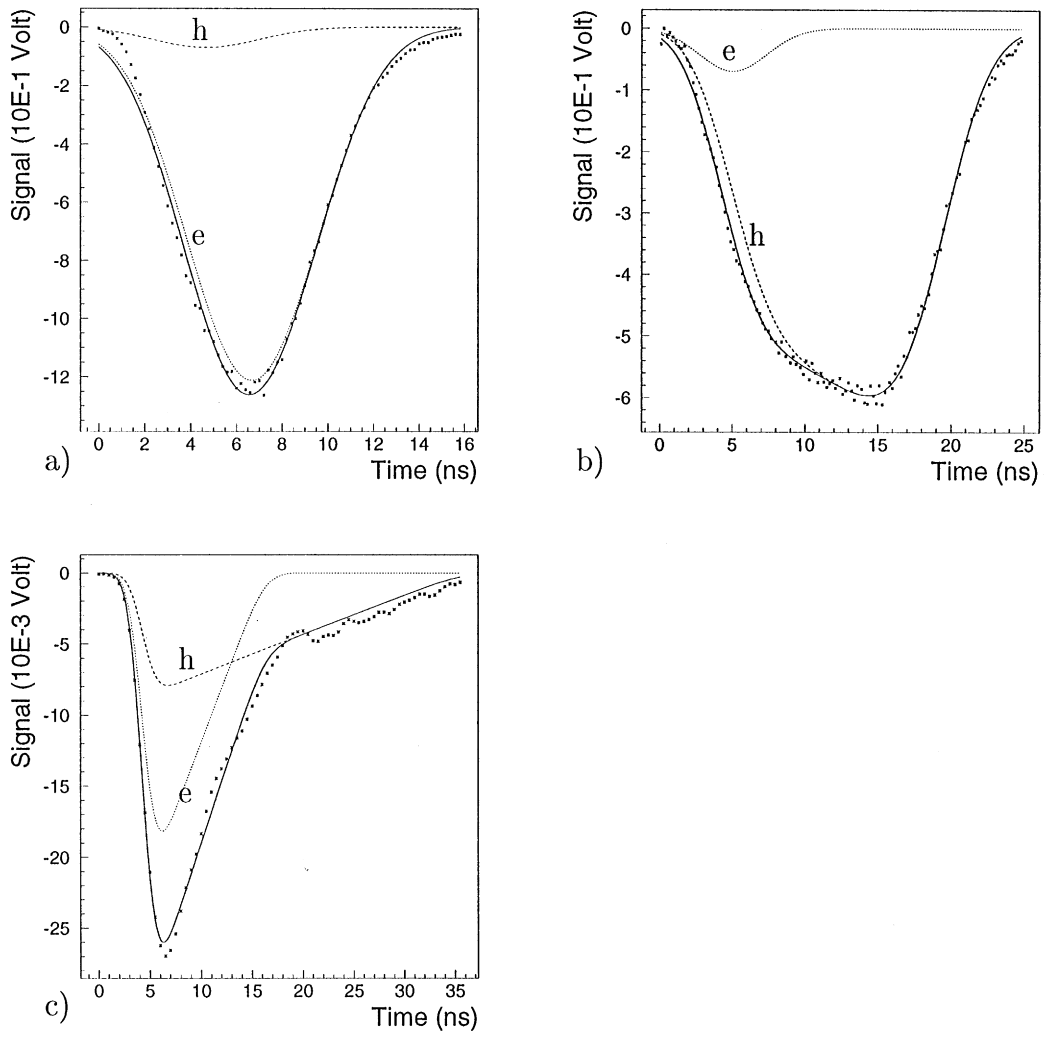


Fig. 3. Fits (full line) of the charge transport model to the current pulse response induced at $\Phi = 0$ by $\alpha$ particles incident on the front side (a), on the back side (b) of detector M25 and by relativistic electrons on detector M50 (c); a bias voltage $V_b = 160$ V is applied in all cases. The individual electron (e) and hole (h) contributions are shown.

in Table 1 are: $\mu_e = 1267 \pm 20$ cm$^2$/V s and $\mu_h = 491 \pm 10$ cm$^2$/V s, respectively.

### 2.2. Irradiated detectors

The detectors were irradiated either with $\approx 1$ MeV neutrons (at the CERN PSAIF), up to a fluence of $9.92 \times 10^{13}$ n/cm$^2$, or with 24 GeV/$c$ protons (at the CERN PS) up to a fluence of $2.87 \times 10^{14}$ p/cm$^2$ (column 6 in Table 1).

The results of the charge transport model fits to the experimental data permit the extraction of the value of $N_{eff}$ as a function of fluence according to

$$N_{eff} = N_0 \exp(-c\Phi) + b\Phi \quad (8)$$

where $N_0$ is the concentration of dopant atoms at $\Phi = 0$, $b$ and $c$ are the acceptor creation and donor removal parameters, respectively. By using Eq. (8) to describe the evolution of $N_{eff}$ with fluence, one obtains the results reported in Table 3. The

Table 2
Electron and hole mobilities of the detectors listed in Table 1, extracted from the model fitted to β and α data at $\Phi = 0$

| Detector | Current pulse source | $\mu_h$ ($cm^2/(V\,s)$) | $\mu_e$ ($cm^2/(V\,s)$) |
|---|---|---|---|
| M4 | α | $503.8 \pm 2.2$ | $1278 \pm 15$ |
| M18 | α, β | $474.4 \pm 2.4$ | $1236 \pm 15$ |
| M25 | α | $476.0 \pm 2$ | $1308 \pm 28$ |
| M35 | α | $472.1 \pm 3$ | $1272 \pm 5$ |
| M49 | β | $546 \pm 11$ | $1266 \pm 24$ |
| M50 | β | $529 \pm 13$ | $1272 \pm 20$ |
| M53 | β | $478 \pm 12$ | $1350 \pm 20$ |
| P88 | α | $459.1 \pm 4$ | $1222 \pm 20$ |
| P189 | α | $480 \pm 20$ | $1340 \pm 27$ |
| P304 | α | $495 \pm 3$ | $1124 \pm 22$ |

difference between $N_{eff}$ reported in Table 1 and $N_0$ of Table 3 is due to the fact that the former value is obtained from the specifications given by the manufacturers, while the latter is the fitted value (Eq. (8)). The results reported in Table 3 show that a silicon detector, initially of n-type, becomes apparently intrinsic around $\Phi_{inv} = 5 \times 10^{12}$ particles $cm^{-2}$ ($\Phi_{inv}$ is the value of the fluence at inversion) and inverts to an apparent p-type for higher fluences, with $N_{eff}$ (Eq. (8)) increasing with fluence. It has to be observed that correlated with the conduction-type inversion, the junction moves from the front side to the back side. As a consequence, for a given bias voltage, the shape of the electric fields depends on the fluence level (Eq. (1)), as does the current induced by the moving charge carriers. The current slope is negative before irradiation, decreases up to $\Phi_{inv}$, changes sign with the conduction-type inversion, and becomes more and more positive with increasing fluence [1].

*2.2.1. α particle data*

Using a simple $pn^+$ junction after the n to p-type inversion (which takes place at a fluence $\Phi \equiv \Phi_{inv} \approx 5 \times 10^{12}$ particles/$cm^2$, a detector with a higher initial resistivity inverting from n to p-type at lower fluence value), the charge carrier transport model reproduces only poorly the measured $V(t)$ as a function of collection time for $\Phi > \Phi_{inv}$, as shown in Fig. 5(a–c) for α particles incident on the back side of detector M4.

In order to fit the data and to account for the evolution of the electrical characteristics of the detectors for fluences beyond $\Phi_{inv}$, the electric field is modified by introducing a 15 μm thick n-type region near the $p^+$ contact (Fig. 4). This double junction concept can also be found in Ref. [7]. This modification of the electric field now permits reproduction of the measured $V(t)$ as a function of collection time for $\Phi > \Phi_{inv}$, as shown in Fig. 5(d–f) for α particles incident on the back side of detector M4. Other examples of results of the fits of the charge transport model, for α particles incident on the front and back side of detector M25, are shown in Figs. 6 and 7. The model applies equally well for the thicker detectors like M35 (508 μm), but no irradiation data were available for the thinner detectors like M53 (see Table 1).

The electron and hole mobilities extracted from the α particle data, after an initial linear decrease with increasing fluence, tend towards a saturation value ($\mu_{sat_{e,h}}$) for fluences beyond $\approx 5 \times 10^{13}$ particles/$cm^2$. The initial decrease is described by

$$\mu_{e,h} = a_{e,h} - b_{e,h} \times \Phi. \quad (9)$$

The saturation values ($\mu_{sat_{e,h}}$) for $\Phi > 5 \times 10^{13}$ particles/$cm^2$ and the coefficients $a_{e,h}$ and $b_{e,h}$ are given in Table 4 for α particle data.

Table 3
Parameters describing the evolution of the effective dopant concentration ($N_{eff}$) with fluence ($\phi$)

| Detector | $N_0$ ($\times 10^{11}$ $cm^{-3}$) | $b$ ($\times 10^{-2}$/(particles cm)) | $c$ ($\times 10^{-11}$ $cm^2$/particles) | $\Phi_{inv}$ ($\times 10^{12}$ $cm^{-2}$) |
|---|---|---|---|---|
| M4 | −2.7 | 1.4 | 9 | ≈8 n |
| M18 | −3.7 | 2.8 | 10 | ≈7 p |
| M25 | −2.2 | 2.5 | 85 | ≈2 p |
| M35 | −2.2 | 2.7 | 76 | ≈2 p |

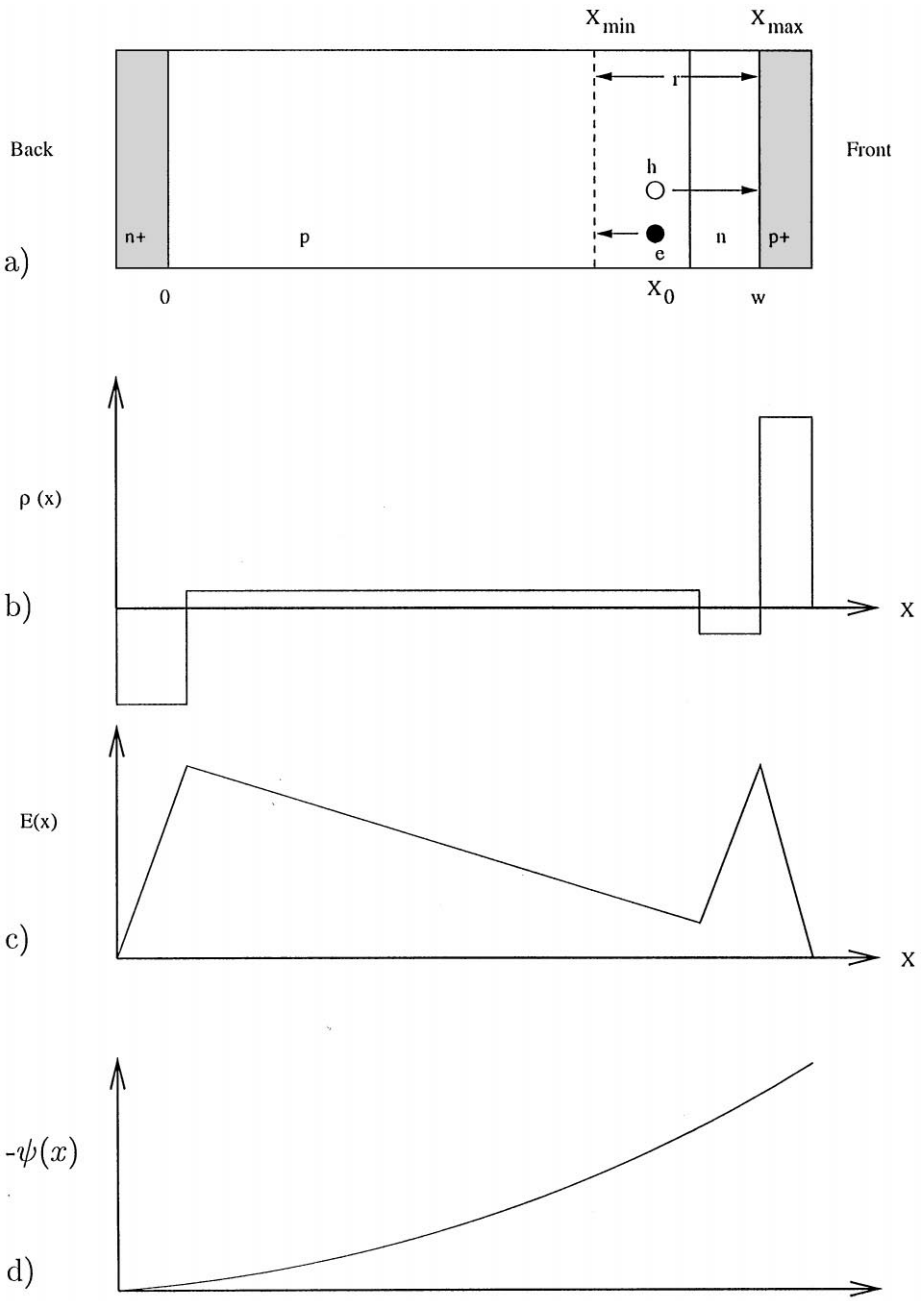


Fig. 4. (a) Representation of a $p^+$–n–p–$n^+$ diode, (b) the dopant profile ($\rho$), (c) the electric field ($E$) and (d) the electrostatic potential ($\psi$).

*2.2.2. β particle data*

The charge transport model was also tested using data obtained from the current pulse response induced by β particles in the non-irradiated (Section 2.1) and irradiated detectors of Table 1. The results of the fits of the charge transport model shown in Fig. 8 for detector M25 are for successive levels of fluence $\Phi$ up to $7.5 \times 10^{13}$ p/cm$^2$.

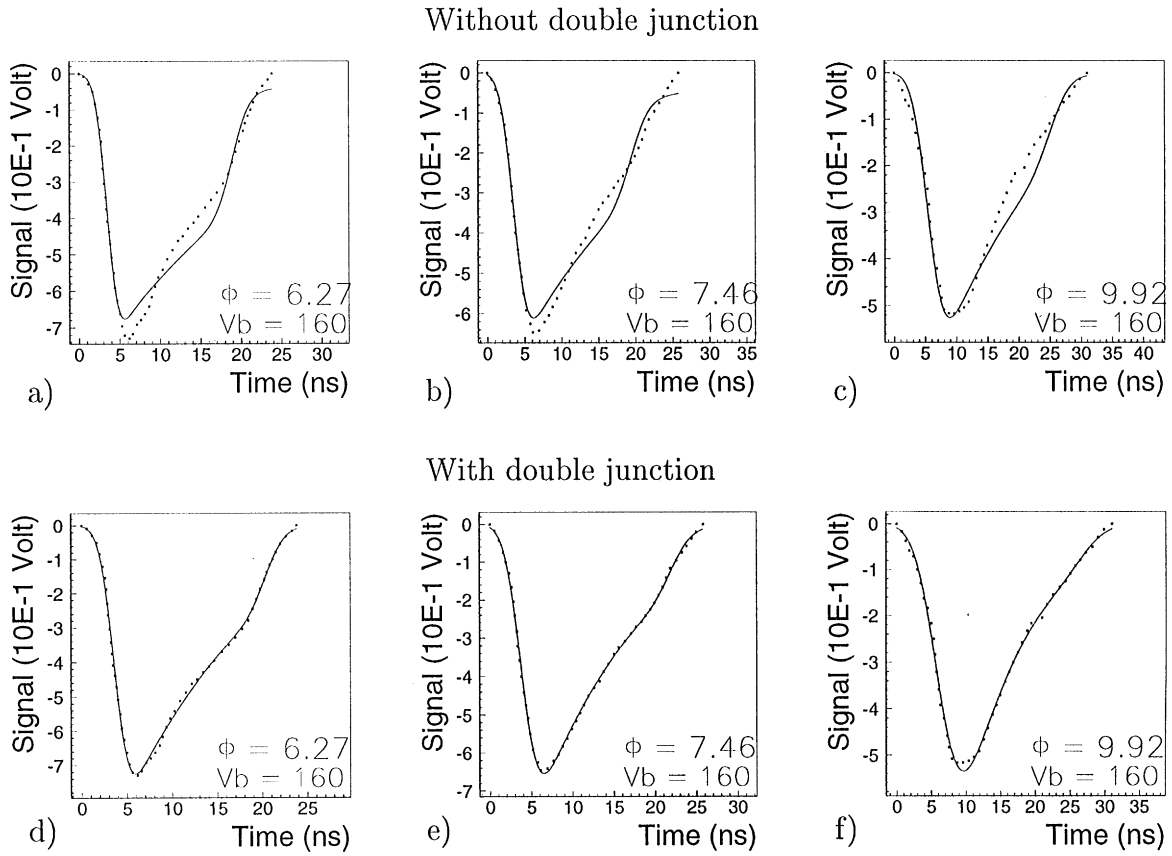


Fig. 5. Fits (full line) of the current pulse response induced by α particles incident on the back side of detector M4: before (a–c) and after (d–f) the introduction of the 15 μm thick n-type junction on the $p^+$ side after inversion at fluences of $\Phi = 6.27$ (a, d), 7.46 (b, e) and $9.92 \times 10^{13}$ n/cm$^2$ (c, f). The bias voltage was 160 V.

Table 4
Parameters describing the evolution of the mobilities with fluence as extracted from data obtained by α particles incident on the front and on the back side and by β particles (Eq. (9) applied to α and β data)

| Detector | $a_h$ (cm$^2$/V s) | $a_e$ (cm$^2$/V s) | $b_h$ (cm$^4$/(particles Vs)) | $b_e$ (cm$^4$/particles Vs)) | $\mu_{sat_h}$ (cm$^2$/V s) | $\mu_{sat_e}$ (cm$^2$/V s) |
|---|---|---|---|---|---|---|
| M4 (α) | 504 | 1200 | 5.6 | 46 | 455 | 990 |
| M18 (α) | 474 | 1195 | 5.3 | 124 | 460 | 1000 |
| M25 (α) | 473 | 1305 | 6.3 | 121 | 460 | 990 |
| M35 (α) | 490 | 1233 | 8 | 115 | 460 | 1000 |
| P88 (α) | 456 | 1176 | 1.6 | 18 | 440 | 1000 |
| P189 (α) | 474 | 1280 | 3.0 | 34 | 450 | 980 |
| P304 (α) | 499 | 1252 | 4.4 | 17 | 452 | 1100 |
| M18 (β) | 481 | 1187 | 14 | 107 | 460 | 1000 |
| M25 (β) | 496 | 1287 | 12 | 113 | 470 | 990 |
| P88 (β) | 428 | 1154 | 3.1 | 7.6 | 395 | 1070 |
| P189 (β) | 460 | 1286 | 0.5 | 23 | 450 | 1050 |
| P304 (β) | 431 | 1270 | 0.3 | 18 | 425 | 1100 |

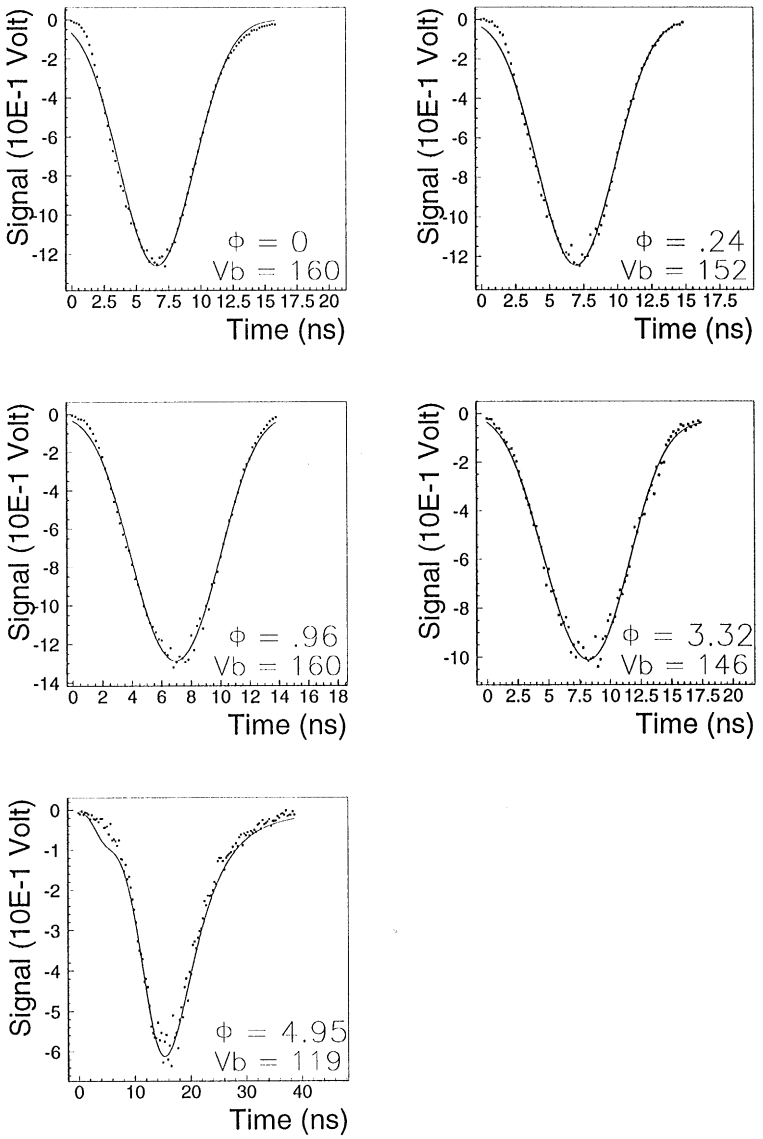


Fig. 6. Fits (full line) of the current pulse response induced by α particles incident on the front side of detector M25 for successive levels of fluence $\Phi$ from 0 up to $4.95 \times 10^{13}$ p/cm$^2$ ($\Phi$ is in units of $10^{13}$ p/cm$^2$, $V_b$ is the applied voltage in volts).

The mobility values extracted from the β data are reported in Table 4. A comparison of the mobility values extracted from α and β data is displayed in Fig. 9(a, b). These figures show that the mobilities (for electrons and holes) extracted from α and β data are in very good agreement, which provides a consistency check of the model.

### 2.3. Charge collection efficiency

As the fluence and thus the number of traps increases, the charge carrier lifetimes due to trapping are found to decrease. The integration of $V(t)$ over the collection time allows one to determine the collected charge. Thus, by comparison of the results

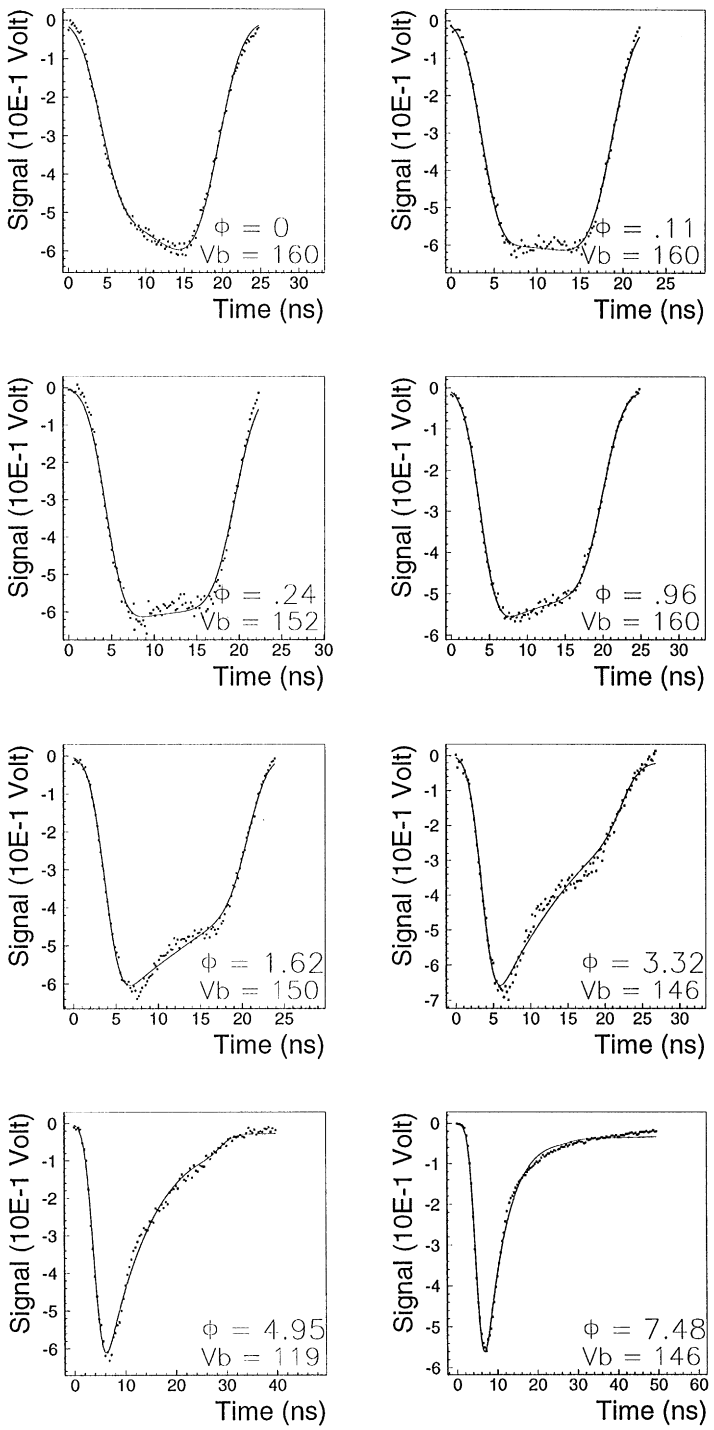


Fig. 7. Fits (full line) of the current pulse response induced by α particles incident on the back side of detector M25 for successive levels of fluence $\Phi$ from 0 up to $7.5 \times 10^{13}$ p/cm$^2$ ($\Phi$ is in units of $10^{13}$ p/cm$^2$, $V_b$ is the applied voltage in volts).

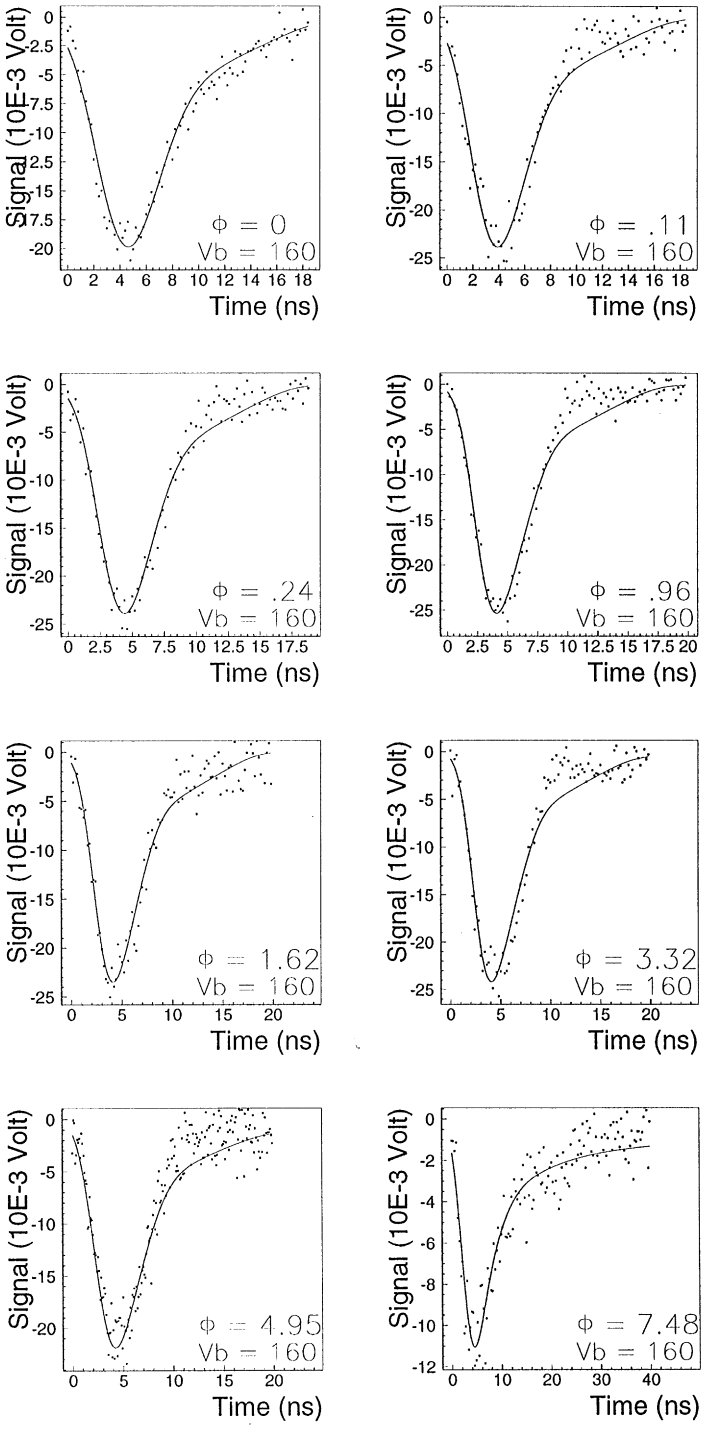


Fig. 8. Fits (full line) of the current pulse response induced by β particles incident on detector M25 for successive levels of fluence $\Phi$ from 0 up to $7.5 \times 10^{13}$ p/cm$^2$ ($\Phi$ is in units of $10^{13}$ p/cm$^2$, $V_b$ is the applied voltage in volts).

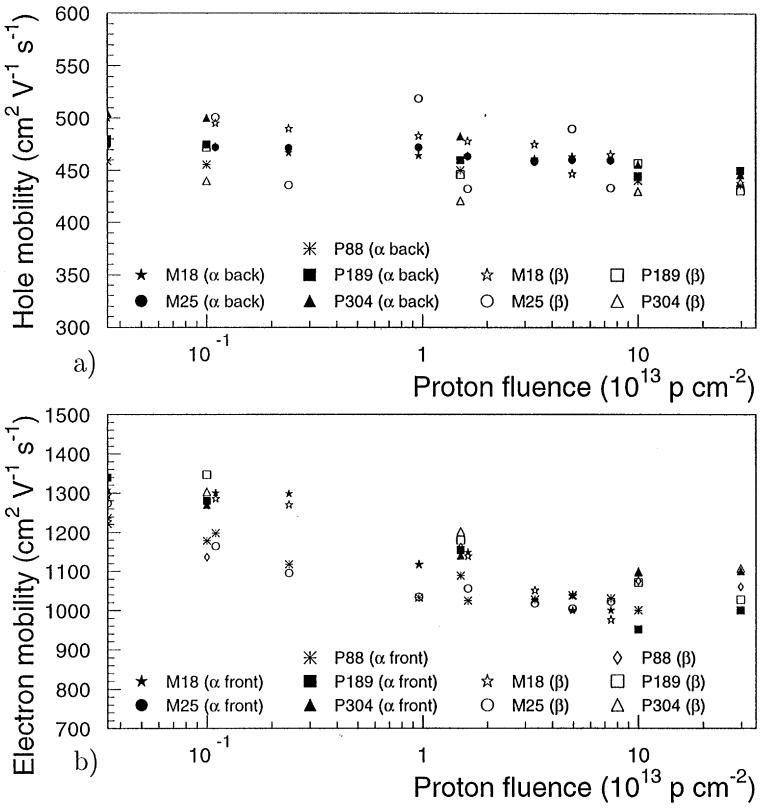


Fig. 9. Comparison of the hole electron (a) and (b) mobilities extracted from α and β particles data using detectors M18, M25, P88, P189 and P304.

obtained using the trapping lifetime extracted at the maximum fluence ($\Phi \approx 10^{14}$ particles/cm$^2$) with those obtained if no trapping had occurred, it is possible to calculate the charge collection deficit. For neutron (proton) irradiated detectors, a charge collection deficit of around 12% (20%) is calculated for α particles incident on the front side and about 18% (30%) for α particles incident on the back side of the detector, for a fluence of $\approx 10^{14}$ particles/cm$^2$. For β particles, a collection deficit of about 13% is calculated for a fluence of $\approx 10^{14}$ particles/cm$^2$. This latter result agrees with the 12% deficit obtained from direct charge collection efficiency (CCE) measurements made with β particles (for a shaping time of 100 ns) [8] in detectors irradiated with fluences $\approx 10^{14}$ particles/cm$^2$. Direct measurements of CCE made with α particles at a fluence of $\approx 10^{14}$ protons/cm$^2$ show a smaller deficit ($\approx 5\%$ on the front side and $\approx 10\%$ on the back side [9]), but these data were recorded with a larger shaping time (1 μs) than the shaping time (100 ns) used in the present work.

## 3. Conclusion

A model describing the transport of the charge carriers generated in n-type silicon detectors by ionizing particles has been presented. To reproduce the experimental current pulse responses induced by α and β particles in non-irradiated and irradiated detectors up to fluences much beyond the n- to p-type inversion, an n-type region 15 μm deep was introduced on the $p^+$ side of the diode. The introduction of this region modifies the electric field after inversion and permits the charge carrier

transport model to reproduce the experimental data up to fluences of $3 \times 10^{14}$ particles/cm$^2$. The physical explanation for introducing this 15 μm deep n-type region (besides the necessity to fit the data) is under evaluation. Several possibilities are considered. Among them is degradation of the ohmic contact which becomes slightly rectifying.

Using this model, the mobilities extracted from data collected with α particles incident on the front and back side of the detectors are found to decrease linearly with increasing fluence up to fluences of around $5 \times 10^{13}$ particles/cm$^2$ and beyond, converging to saturation values of about 1000 and 450 cm$^2$/V s for electrons and holes, respectively. The mobility values extracted from the β data for the same detectors are found to be in very good agreement with the mobilities extracted from data collected with α particles. This agreement provides a consistency check of the model.

The charge carrier lifetime degradation due to more trapping with increased fluence is responsible for a predicted charge collection deficit which is found to agree with the charge collection deficit measured directly with β and α particles.

## References

[1] C. Leroy et al., Nucl. Instr. and Meth. A 426 (1999) 99
[2] H.K. Gummel, IEEE Trans. Electron. Devices ED-11 (1964) 455.
[3] S. Ramo, Proc. IRE 27 (9) (1939) 584.
[4] Application Software Group, CERN Program Library D506, MINUIT Function Minimization and Error Analysis, 1992.
[5] P. Roy, Étude de la réponse en courant de détecteur silicium opérés en environnement de très hautes radiations, M.Sc. Thesis, Université de Montréal, 1994.
[6] C. Leroy et al., Nucl. Instr. and Meth. A 388 (1997) 289.
[7] Z. Li, H.W. Kraner, J. Electron Mater. 21 (7) (1992) 701.
[8] C. Leroy et al., Study of electrical properties and charge collection of silicon detectors under neutron, proton and gamma irradiations, in: A. Menzione, A. Scribano (Eds.), Proceedings of the Fourth International Conference on Calorimetry in High Energy Physics, La Biodola, Isola d'Elba, Italy, 19–25 September 1993, World Scientific, Singapore, 1994, p. 627.
[9] S. Pospisil, talk given at this conference.